Assimilating WIVERN winds in WRF model: an application to the outstanding case of the Medicane Ianos

Stefano Federico[1], Rosa Claudia Torcasio[1], Claudio Transerici[1], Mario Montopoli[1], Cinzia Cambiotti[2], Francesco Manconi[2], Alessandro Battaglia[2], and Maryam Pourshamsi[3]

[1]CNR-ISAC, via del Fosso del Cavaliere 100, 00133 Rome
[2]Dipartimento di Ingegneria dell'Ambiente, del Territorio, Politecnico di Torino, Turin, Italy
[3]ESA-ESTEC, Noordwijk, Netherlands

Abstract. Accurate weather forecasts are important to our daily lives. Wind, cloud and precipitation are key drivers of the Earth's water and energy cycles, and they can also pose weather-related threats, making the task of numerical weather prediction (NWP) models particularly challenging and important.

The Wind Velocity Radar Nephoscope (WIVERN) mission will be the first space-based mission to provide global in-cloud wind measurements, and also the first to deliver simultaneous observations of winds, clouds and precipitation. The mission is proposed as a candidate for the European Space Agency (ESA)'s Earth Explorer 11 within the Future Earth Observation (FutureEO) programme. It is currently in Phase A, with the recommendation decision expected in July 2025. If the mission is successfully selected for implementation, its data could be beneficial to several sectors: improving our knowledge of weather phenomena, validate climate statistics, and enhancing NWP performance. This paper aims to contribute to the last point by analyzing the impact that WIVERN would have in the case of a Tropical-like cyclone (TLC) event.

In this work, the impact of assimilating WIVERN Line of Sight (LoS) winds (retrieved from WIVERN Doppler measurements) on NWP performance is assessed, for the high-impact case study of Medicane Ianos, which occurred in mid-September 2020 in the central Mediterranean and made landfall on the west coast of Greece.

To this end, we generate WIVERN pseudo-observations, that are assimilated in the Weather Research and Forecasting (WRF) model run at moderate horizontal resolution (4 km).

Results show that assimilating WIVERN into the WRF model has a positive impact on the prediction of the Medicane trajectory. Specifically, assimilating WIVERN just once improves the trajectory forecast error by 43%. The data assimilation of WIVERN pseudo-observations affects not only the storm's trajectory but also its physical characteristics. It is also shown that the assimilation improves the prediction of precipitation and surface winds, and has the potential to improve our resilience to severe weather events by enabling better forecasts of storm impacts. Finally, we present the results of two sensitivity experiments in which the background and observation errors were different. The results show greater sensitivity to changes in the background error matrix.

1 Introduction

Numerical weather prediction (NWP) is an initial and boundary condition problem, and its performance depends on an accurate representation of the initial atmospheric state. The purpose of data assimilation is to find a model state that provides the best match between the most recent model prediction and the available observations. This model state, called the analysis, can then be used to start a new model forecast with improved initial conditions.

In this context, wind observations are particularly important to assimilate in NWP in order to improve the forecast (Baker et al., 2014; Horányi et al., 2015; Li et al., 2023; Federico, 2013).

Between 2018-2023, the European Space Agency (ESA)'s Aeolus satellite provided wind observations along the Horizontal Line of Sight (HLoS) through atmospheric columns in optically thin clouds and clear sky, using a Doppler Wind Lidar. The positive impact of Aeolus data assimilation in NWP models has been demonstrated by major meteorological centers (Rani et al., 2022; Garrett et al., 2022; Martin et al., 2023; Rennie et al., 2021). Aeolus observations have also been assimilated in limited-area NWP models, showing, albeit to a lesser extent compared to global models, a positive impact (Stathopoulos et al., 2023; Matsangouras et al., 2023; Hagelin et al., 2021; Feng and Pu, 2023).

The WInd VElocity Radar Nephoscope (WIVERN) Illingworth et al. (2018); Battaglia et al. (2022); Tridon et al. (2023)) has been selected by ESA as one of the two Earth Explorer 11 candidates. WIVERN, will carry a 94 GHz radar with a conically scanning 800 km swath. It will provide, for the first time, profiles of in-cloud winds and precipitation on a global scale, with a revisit time of 1.5 days at the equator. The implications of this unprecedented sampling capability have been recently discussed in Tridon et al. (2023); Scarsi et al. (2024a). WIVERN measurements will have a vertical resolution of approximately 600 m and an instantaneous footprint of less than 1×1 km^2 (Illingworth et al., 2018). Wind measurements will then be averaged along the scanning direction over 5 km or more to reduce measurement noise.

The focus of this paper is to study, for the first time, the impact of assimilating WIVERN in-cloud winds in the Weather Research and Forecasting (WRF) model (Skamarock et al., 2019) for a high impact storm occurred in the Mediterranean Sea. To robustly assess the impact of WIVERN wind data assimilation (DA) on WRF forecasts, we use an ensemble data assimilation (EDA) framework (Tan et al., 2007; Harnisch et al., 2013).

Mediterranean cyclones are key features of the region's climate and water cycle (Flaounas et al. (2022); Ali et al. (2023)). These cyclones are driven by the large-scale extra-tropical circulation and Rossby wave breaking, and they involve contributions from both dry dynamic and moist diabatic forcings (Flaounas et al., 2021; Raveh-Rubin and Wernli, 2016; D'Adderio et al., 2022; Lfarh et al., 2023). Among Mediterranean cyclones, a special class, known as Medicanes (Mediterranean Hurricanes, Emanuel (2005)), has attracted considerable attention of both the scientific community and the public. For the broader public, these storms are important due to their high destructive power. From a scientific point of view, they are of interest because they show tropical characteristics such as a symmetric structure, a cloud-free centre resembling an eye, and a warm core extending at least partially through the troposphere (D'Adderio et al., 2022; Di Francesca et al., 2025). There are many studies on Medicanes (Fita and Flaounas (2018); Miglietta and Rotunno (2019); Dafis et al. (2020), that examine the physical characteristics of these storms and the key role of deep convection in the formation of the deep warm core. Among this type of storm, we selected

Medicane Ianos as a case study. This Medicane, was among the most intense Medicanes in the Mediterranean (Lagouvardos et al., 2022; D'Adderio et al., 2022), occurred in mid-September 2020 and impacted Greece with strong winds, heavy precipitation, and storm surges during landfall (Ferrarin et al., 2023; Androulidakis et al., 2023). Ianos was used in several studies to investigate various aspects of the storm, including the influence of convective parameterisation and microphysical characteristics (Saraceni et al., 2023; Comellas Prat et al., 2021), the impact of the sea surface temperature on storm evolution (Varlas et al., 2023) as well as diabatic forcing and storm surge impact (Sanchez et al., 2023; Ferrarin et al., 2023).

Recently, Pantillon et al. (2024) published a model inter-comparison of Medicane Ianos simulations, as part of the COST Initiative CA19109 "MedCyclones: European Network for Mediterranean Cyclones in weather and climate". They compared 10 different modeling systems, including different WRF model configurations, for storm track prediction. The study highlighted the importance of explicitly resolving convection in the simulation of the storm, which plays a fundamental role for accurately simulating cyclone track and storm deepening. It also found a spread among the ensemble members, with most models predicting a storm track shifted southward compared to the best estimate (Flaounas et al., 2023). In this paper, as in Pantillon et al. (2024), we use storm track as a primary metric to study the impact of WIVERN winds DA in the WRF model.

The paper is organized as follows: Section 2 present the WRF model configuration, the ensemble framework, and the methodology used to generate pseudo-observations for the case study. Section 3 shows the results of WIVERN winds data assimilation on prediction of the Medicane Ianos trajectory and other storm parameters, as well as its impact on rainfall and surface wind prediction. This section also includes two sensitivity tests on the choice of background and observation error matrices. Conclusions are provided in Section 4. Appendix A gives further details on the assimilation of WIVERN winds using three-dimensional variational data assimilation (3DVar).

2 Data and Methods

2.1 WRF model settings

In this work, we use the WRF model 4.1 with 400 grid points in both the west-east (WE) and south-north (SN) directions, and 55 vertical levels extending from the surface to 50 hPa (Skamarock et al. (2019)). The model horizontal resolution is 4 km in both WE and SN directions, and the domain covers the Central Mediterranean basin. The center of the domain is located at $(15°E, 40°N)$, with the SW and NE corners at $(6°E, 35°N)$ and $(23°E, 46.6°N)$, respectively (see Figure 9). The physical parameterisation used in the model include the Thompson microphysics scheme (Thompson et al. (2008)), the Mellor-Yamada-Janjic turbulent kinetic energy boundary layer scheme (Janjic (1994)), the Dudhia scheme for shortwave radiative transfer (Dudhia (1989)), and the Rapid Radiative Transfer Model (RRTM) for longwave radiation Mlawer et al. (1997)).

Initial and boundary conditions (IC/BC) are taken from the European Centre for Medium-range Weather Forecast - Ensemble Prediction System (ECMWF-EPS) of the Integrated Forecasting System (IFS) run issued at 12:00 UTC on 16 September 2020. The ECMWF-EPS consists of one unperturbed (control) member and 50 perturbed members, resulting in a total of 51 WRF runs nested within the ECMWF-EPS initial and boundary conditions.

2.2 Methodology

The simulations start at 12 UTC on 16 September 2020 and end at 12 UTC on 18 September 2020. Two different data assimilation cycles are considered: a 3-hourly cycle and a 24-hourly cycle. In the 3-hourly cycle, referred to as WIV_{3h}, WIVERN winds along the LoS are assimilated every 3h. Although WIVERN will have a longer repetition cycle, this 3h experiment is used to assess the effectiveness of WIVERN wind data assimilation under idealized conditions, assuming the satellite operates in a constellation formation. Hereafter, "WIVERN winds DA" refers to the assimilation of WIVERN in-cloud winds measured along the line of sight.

In the 24h cycle, referred to as WIV_{24h}, a single assimilation of WIVERN winds is performed at 12 UTC on 17 September. This setup is designed to represent a more realistic scenario, in which WIVERN overpasses a mature storm system. Finally, a control ensemble, $CTRL$, is also included. This ensemble is run without any data assimilation, using only different initial and boundary conditions derived from the ECMWF-EPS. Each WRF ensemble member corresponds directly to the ECMWF-EPS member that provides its IC/BC.

For the data assimilation, we use the 3DVar developed by Federico (2013), based on the framework by Barker et al. (2004) (see also Torcasio et al. (2024) for recent developments of the 3DVar software). The background error matrix is computed form the $CTRL$ ensemble members at 12 UTC on 17 September 2020 by:

$$\mathbf{B} = \mathbf{X}\mathbf{X}^{\mathbf{T}} \tag{1}$$

$$\mathbf{X} = \frac{1}{(N_{ens}-1)^{1/2}}(\mathbf{x_{b1}} - \overline{\mathbf{x^b}}, \mathbf{x_{b2}} - \overline{\mathbf{x^b}}, ..., \mathbf{x_{N_{ens}}} - \overline{\mathbf{x^b}}) \tag{2}$$

where N_{ens} is the number of ensemble members and $\overline{\mathbf{x^b}}$ is the ensemble average. Further details about the background error matrix and its implementation in the 3DVar are given in Appendix A. For a complete reference, the reader is referred to Federico (2013) and Barker et al. (2004).

To evaluate the impact of WIVERN Doppler data assimilation, we adopted the following steps:

- First, we generated an ensemble of the WRF model nested in the ECMWF-EPS of the IFS, starting at 12 UTC on the 16 September 2022 ($CTRL$ ensemble);
- From the $CTRL$ ensemble, we selected a representative member, which is the one whose simulated storm track is in closest agreement with the best a-posteriori estimate of Ianos' trajectory provided by Flaounas et al. (2023);
- We then generated pseudo-observations of WIVERN winds using the simulator developed by Da Silva et al. (2025) (see also Battaglia et al. (2022)). The simulator was applied to the output of the representative member. One WIVERN

pseudo-observation was generated every 3h, from 15 UTC on 16 September to 09 UTC on 18 September. These pseudo-observations consist of WIVERN winds along the LoS. Considering WIVERN conically scanning geometry, the LoS pseudo observations are given by:

$$f(U,V,W) = U\sin\theta\cos\phi + V\sin\theta\sin\phi + W\cos\theta \tag{3}$$

where θ is the angle between the WIVERN antenna and the vertical direction $(41°)$, ϕ is the azimuth, and U,V,W are the zonal, meridional and vertical wind components. Assimilation is done in stratiform areas where W is negligible. For these areas the WIVERN winds along the LoS are given by:

$$f(U,V) = U\sin\theta\cos\phi + V\sin\theta\sin\phi \tag{4}$$

When generating WIVERN pseudo-observations, we assume that the Medicane is well sampled by WIVERN. Figure 1 shows the best a-posteriori estimated trajectory of Ianos, the representative member trajectory and the conical scan of WIVERN at 12 UTC on 17 September 2020. The assumed satellite ground track is shown in Figure 1 for all scenes used for generating pseudo-observations. With this assumption, the Ianos trajectory center is well inside the radar swath, and the Medicane is well sampled by WIVERN.

2.3 Representative member choice and pseudo-observations

Figure 2 shows the 51 trajectories of the Medicane Ianos, simulated by the WRF runs nested within the 51 members of the ECMWF-EPS. Each trajectory is defined by tracking the position of minimum sea-level pressure around the area of the Medicane. The color bar corresponds to the colors of the segments joining two dots and indicates the pressure at the initial point of each segment (there are three segments between two dots). The dots, plotted every 3h, correspond to the position of the system at different times. As expected, the trajectories are initially close to each other, but diverge with time, due to the amplification of small differences in the initial conditions by the evolving atmospheric flow. The red line in 2 shows the best estimated trajectory. According to the best estimate, Medicane Ianos made landfall between the islands of Zakynthos and Kefalonia (Lagouvardos et al. (2022)). However, the pressure of the best estimated trajectory remains too high ($>$ 1000 hPa), compared to the observations from the Palliki meteorological station on Kefalonia island, which recorded a minimum pressure of 984 hPa (at 05 UTC on 18 September). This discrepancy is because the reference trajectory is derived from the ERA5 reanalyses. Therefore, we only considered the trajectory, i.e. the position of the surface minimum pressure, and not the sea level pressure values, when comparing the WRF ensemble trajectories of the Medicane Ianos with the reference trajectory.

As shown in Figure 2, most simulated trajectories are displaced to the south of the best estimated trajectory. This result is in agreement with that of Pantillon et al. (2024), showing that the forecast of the Ianos trajectory of several meteorological models is to the south of the best estimated trajectory.

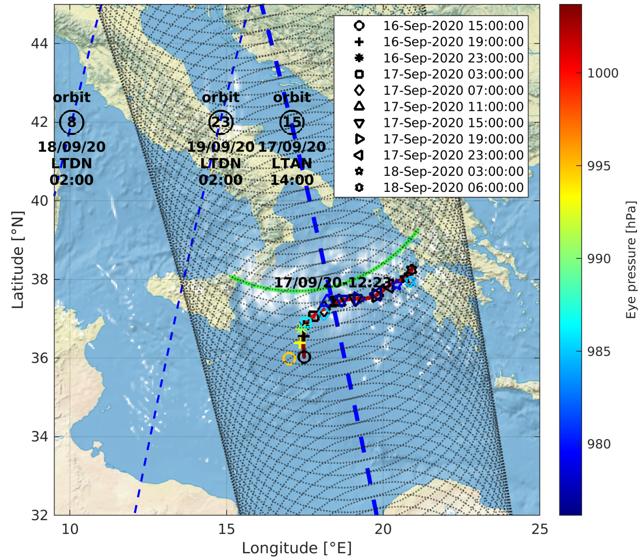

Figure 1. WIVERN track for the Medicane Ianos. The a-posteriori best estimated trajectory is shown by the red-line, the reference trajectory is shown by symbols. The time range of the trajectories is indicated in the legend. The surface pressure along the track is shown by the color (both line and marks). The WIVERN sub-satellite point is represented by the blue dashed line, while the radar conical scan is shown by the gray dashed line, showing the 800 km wide swath. Times are indicated in local time (UTC+2h) ascending/descending node. The passages of WIVERN over the area would have occurred at 00 UTC on 18 and 19 September 2020 and at 12 UTC on 17 September 2020, however, only the 12 UTC observations would have sampled Ianos at about the center of the scene.

The representative member of the WRF ensemble was selected by minimizing the average distance between the members and the best estimated trajectory. This average distance is calculated as:

$$d_{be,m}(t) = |\boldsymbol{r_{be}}(t) - \boldsymbol{r_m}(t)| \tag{5}$$

$$\bar{D} = \sum_{t=1}^{T} \sum_{m=1}^{M} \frac{d_{be,m}(t)}{TM} \tag{6}$$

where $\boldsymbol{r_m}$ and $\boldsymbol{r_{be}}$ are the position vectors of the minimum sea-level pressure of the m-th ensemble member and the best estimated trajectory, respectively, at time t. The distance of the whole ensemble from the best estimated trajectory is given by averaging $d_{be,m}$ over all ensemble members M and forecast times T. The trajectory error was computed over the period from 15 UTC on 16 September 2020 to 06 UTC on 18 September 2020, based on hourly WRF output. This time range was chosen considering two requirements: a) the simulation starts at 12 UTC on 16 September, and the minimum pressure at this initial time is determined by the ECMWF-EPS initialisation rather than the WRF evolution; b) after 06 UTC on 18 September, many ensemble members made their landfall. To simplify the analysis, we consider the trajectory of the Ianos evolution over the Ionian Sea.

Figure 3, panel a), shows a histogram of the distances between each member of the $CTRL$ ensemble and best estimated trajectory from Flaounas et al. (2023). The smallest distance, 30.0 km, is achieved by member 42, while the largest, 101.2 km, by member 11. Figure 3, panel b), shows the trajectory of member 42 together with the best estimated trajectory (i.e. the same trajectories of Figure 1). It is apparent that this member follows well the best estimated trajectory of Ianos. According to the results, member 42 is chosen as the representative member and is used to generate pseudo-observations of the Medicane Ianos, as if it was observed by WIVERN. We computed pseudo-observations every 3 h, for a total of 15 WIVERN scenes, from 15 UTC on 16 September to 09 UTC on 18 September. This was done by applying the WIVERN simulator (Da Silva et al. (2025);Battaglia et al. (2022)) to the member 42 output files, and assuming that the Ianos Medicane is well sampled by WIVERN. From now on, the member 42 represents our truth, i.e. the simulation to reproduce when applying WIVERN winds DA to other ensemble members.

Figure 4 panel a), shows the number of pseudo-observations available at different vertical levels at 12 UTC on 17 September, which is the time when WIVERN winds are assimilated in WRF for WIV_{24h}. The largest number of observation is at 7 km height, which decreases at higher levels due to the reduced optical thickness of clouds, and at lower levels due to radar signal attenuation.

Figure 4 panel b) shows the observation error (black curve) and the model errors (blue curve) as functions of altitude. The observation error, σ^2_{LoS}, decreases with increasing signal to noise ratio, as discussed in Battaglia et al. (2025b). For WIVERN, the observation error is given by:

$$\sigma^2_{LOS} = \frac{1}{N}\frac{v^2_{Nyq}}{2(\pi\beta)^2}\left[\left(1+\frac{1}{SNR}\right)^2 - \beta^2\right] \tag{7}$$

$$SNR = 10^{\frac{Z-Z_{min}}{10}}; \quad \beta = e^{-\frac{1}{2}\frac{\pi^2\sigma_v^2}{v^2_{Nyq}}}; \quad v_{Nyq} = \frac{\lambda}{4T_{HV}}$$

where $\lambda = 3$ mm is the radar wavelength, $T_{HV} = 20\mu s$ is the separation between the two polarized pulses H and V, $N = 40$ is the number of pulse pairs, σ_v =4 ms^{-1} is the Doppler spectral width, v_{Nyq} is the Nyquist velocity, and $Z_{min} = -15$ dBZ. The σ^2_{LOS} does not take into account errors like non uniform beam filling, wind shear, and mispointing errors (Scarsi et al. (2024b)). These errors are expected to be lower than 1 ms^{-1} (Battaglia et al. (2022); Tridon et al. (2023); Battaglia et al. (2025a)). To account for these errors the corrected σ^2_{LOS} is:

$$\sigma^2_{cLOS} = \sigma^2_{LOS} + c_1^2 \tag{8}$$

with $c_1 = 1$ ms^{-1}.

Figure 4 panel b) shows that the model error is larger than the observation error; this suggests a large impact of WIVERN data assimilation for the Ianos case study. To study the sensitivity of the results to the assumed observation error, Section 3 presents an experiment with the observation error inflated to match the model error. As for the 3DVar framework, the observation error for each measurement is computed following the Eqn. (7-8). The observation error matrix is assumed diagonal, i.e. we neglect the error correlation among different observations. WIVERN pseudo observations are generated with the WIVERN simulator

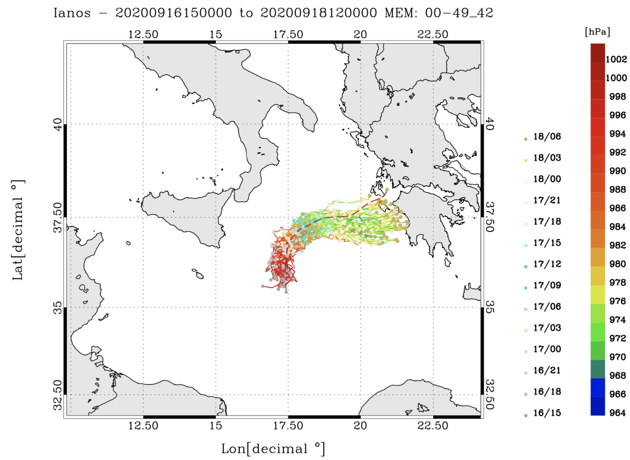

Figure 2. Trajectories followed by the ensemble members of the WRF control ensemble.

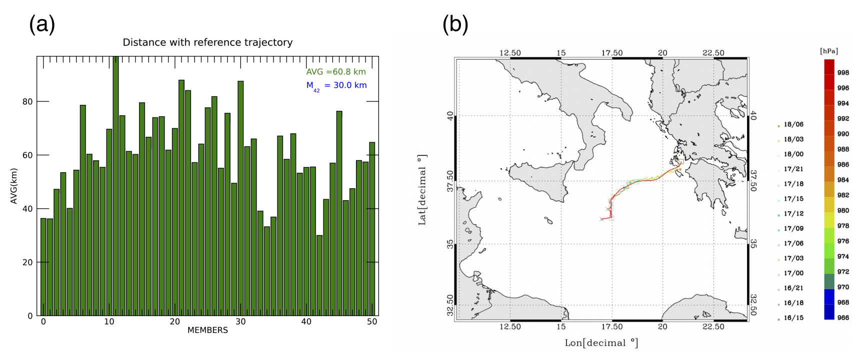

Figure 3. a) Histogram of the distances between the WRF ensemble members at the Ianos best estimated trajectory. The average distance is 60.8 km, while the minimum distance is achieved by the member 42 (30.0 km); b) trajectories of the best a-posteriori estimated trajectory of Ianos (red curve) and the representative member 42.

with an horizontal resolution of 5 km, and they are thinned to 10 km to account, at least partially, for assuming a diagonal observation matrix.

3 Results

After generating pseudo-observations, we performed a run of the whole ensemble assimilating WIVERN pseudo observations every 3 h. The result is shown in Figure 5. The assimilation of WIVERN winds every 3 h has a very important impact on the Ianos trajectory. First, all the trajectories are now focused along the trajectory of the representative member 42, which is shown in black (and without dots for clarity). Second, the landfall occurs in the northern part of the Peloponnese with many member

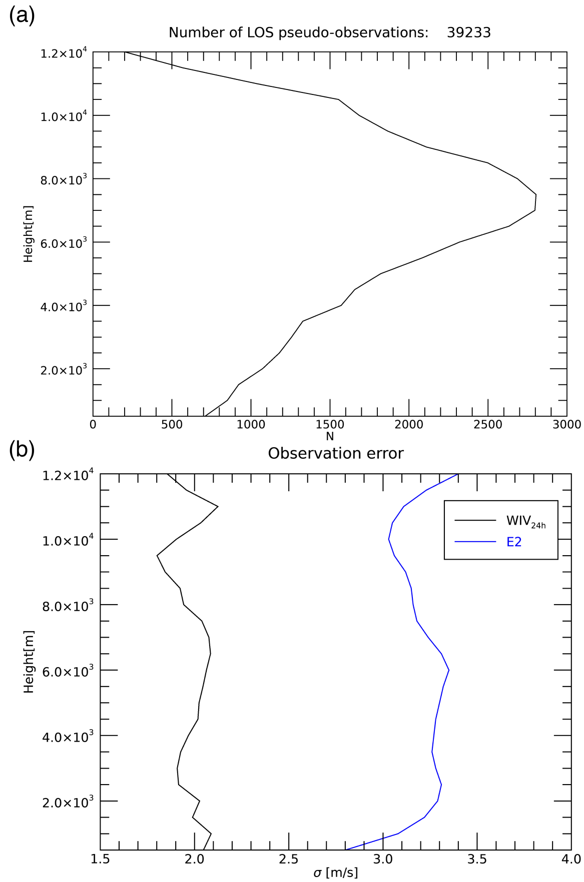

Figure 4. a) Vertical distribution of the number of WIVERN observations; b) Vertical average of the observations' error (black curve) and of the model error (blue curve). The model error is also used as observation error in the sensitivity experiment with inflated observation error.

crossing the Zakynthos island or passing in the gap between the Kefalonia and Zakynthos islands. The distance of the ensemble from the member 42, computed by Eqn. (5-6) is 14.9 km, to be compared with 62.5 km of the $CTRL$ ensemble. Importantly, changes in the winds caused by the WIVERN winds DA are propagated, through the model physics, to other parameters, focusing the ensemble members towards the representative member 42. This point is demonstrated for the minimum sea level pressure in Figure 6, with the spread of the minimum sea level pressure substantially reduced by the WIVERN winds DA. It is also noted the increase of the minimum sea level pressure of the WIV_{3h} compared to the $CTRL$ ensemble forecast as many members of the $CTRL$ ensemble were predicting a pressure lower than the member 42 and this is improved by WIVERN winds DA.

Hereafter we focus on the WIV_{24h} numerical experiment and two sensitivity tests. In these experiments, data assimilation is done at 12 UTC on 17 September for each member of the ensemble, then follows a 24 h forecast. WIV_{24h} represents a

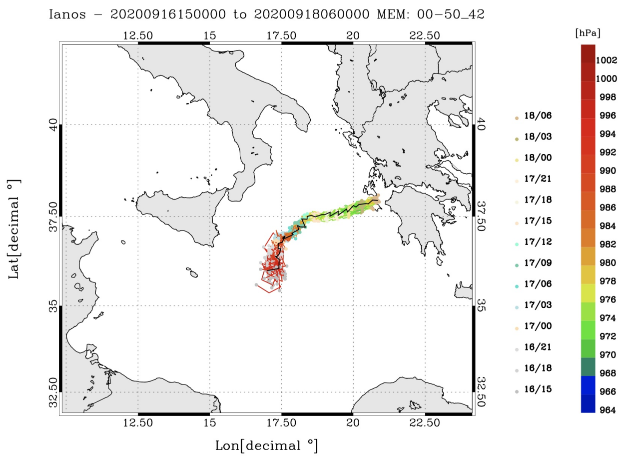

Figure 5. Trajectory followed by the WRF ensemble when WIVERN DA is applied every 3 h. The member in black is the representative member 42.

realistic scenario in which WIVERN sample Ianos one-time in the period of the simulations considered in this paper. Indeed, considering the 1.5 day revisiting time at the equator of WIVERN, the Ianos Medicane would have been sampled two times (Figure 1) in the time window considered in this work, but the second time would have been too close to the landfall for the forecasting purposes of this paper.

The trajectories of WIV_{24h} ensembles are shown in Figure 7. By comparing Figure 7 and Figure 2, it is apparent the positive impact of WIVERN DA on the forecast of the Ianos trajectory. In particular, the $CTRL$ forecast shows several trajectories going towards the southern part of the Peloponnese; these trajectories are shifted northward in the experiments with WIVERN DA, even if the WIV_{24h} trajectories still tend to go to the south of the member 42 trajectory. Another interesting point is the increase in pressure along the final part of the trajectories compared to the $CTRL$ ensemble. This is shown by the yellow-green colors of the segments in the last part of the trajectories in Figure 7, compared to the green colors of the same traits in Figure 2. This difference is attributed to the change in the storm dynamics after DA, and to the WRF model physics, that propagates changes in the wind field to the mass fields through physical relationships.

In Figure 7, the violet arrow indicates the time of analysis. It is interesting to note that the trajectories converge following the analysis, as the different ensemble members tend towards the representative member 42. These results are summarized in Table 1, for the period 12 UTC on 17 September to 06 UTC on 18 September, showing the average distance of the ensemble from the member 42 for the $CTRL$ and WIV_{24h} ensembles. The table also includes the skill of the WIV_{24h} ensemble compared to the $CTRL$ ensemble. The skill score, $I(\%)$, is given by:

$$I(\%) = 100\frac{\bar{D}_{CTRL} - \bar{D}_{exp}}{\bar{D}_{CTRL}} \quad (9)$$

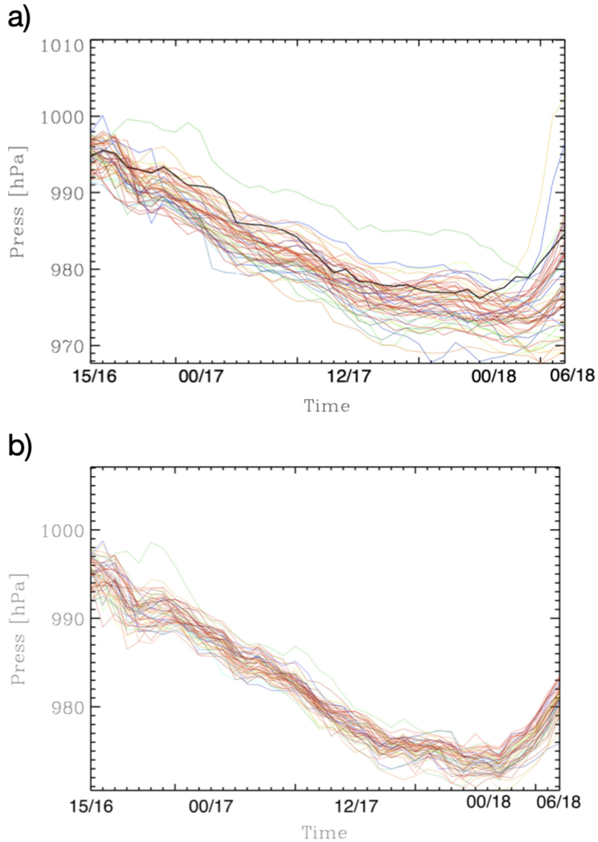

Figure 6. Time variation of minimum sea level pressure for a) the background ensemble; b) the WIV_{3h} experiment. The black line in panel a) is the minimum sea level pressure of member 42.

where $\bar{D}$ is given by Equation (6) and exp can be $3h$ or $24h$.

It is interesting to examine the trajectory error as a function of the ensemble member (i.e. Eqn. 6 without averaging over members) and as a function of time (i.e. Eqn. 6 without averaging over time). These statistics are shown in Figure 8. Considering the error as a function of ensemble member, there are a few points to note. First, the WIV_{3h} ensemble performs better than $CTRL$ across all members, the only exception being member 34, for which the improvement is very small. This shows that assimilating WIVERN every $3h$ gives a strong constraint on storm evolution for all the members. Assimilating WIVERN only once (WIV_{24h}) still has a positive impact on the simulation of the Medicane Ianos' trajectory, with the error reduced for almost all members. Sometimes, the error is substantially reduced, as for the member 11 (and many others), sometimes the improvement in the trajectory forecast is small, as for member 47, and few times there is a negative impact of assimilating WIVERN winds, as for member 35. However, the positive impact is very important for some members, with the trajectory error halved in some cases and improvements often larger than $15-20$ km, and, when there is a negative impact of assimilating

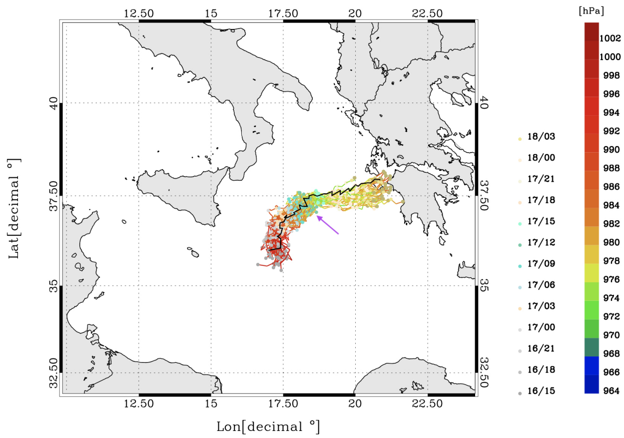

Figure 7. Trajectories followed by the members of the WRF ensemble WIV_{24h}. The trajectory in black is the representative member 42, while the violet arrow indicates the assimilation time.

Table 1. Average distances of the ensemble members from the member 42, and improvement ($\%$) with respect to $CTRL$ ensemble.

EXP	$Err(km)$	$I(\%)$
$CTRL$	62.5	/
WIV_{24h}	35.4	43
WIV_{3h}	14.9	64

WIVERN winds, it is less than 10 km.

Member 34 deserves a special mention, as WIVERN DA does not improve its trajectory forecast. As shown in Figure 8 panel a), this member already has a very low background error (about 10 km), leaving little room for further improvement through data assimilation.

Overall, the analysis of Figure 8, panel a), leads to three main conclusions: a) assimilation of WIVERN winds along the LoS improves the forecast of the Ianos trajectory; b) the magnitude of the improvement varies depending on the ensemble member; and c) the negative impact of WIVERN DA is limited to few cases and less than 10 km, while the positive impact is often larger than $> 15-20$ km. In addition, while the improvement of WIVERN DA is dependent on the member, this dependence is greatly reduced if WIVERN is assimilated every 3 h, showing the ability of WIVERN to substantially change the storm evolution, when frequently assimilated.

Figure 8 panel b) shows the trajectory error as a function of forecasting time from 15 UTC on 16 September to 06 UTC on 18 September. The error of the $CTRL$ ensemble increases with the forecast time, as expected. The WIV_{24h} forecast differs from the $CTRL$ forecast after the analysis (12 UTC on 17 September), however, the improvement is large and lasts until the end of the period considered, showing a long-lasting effect of WIVERN DA.

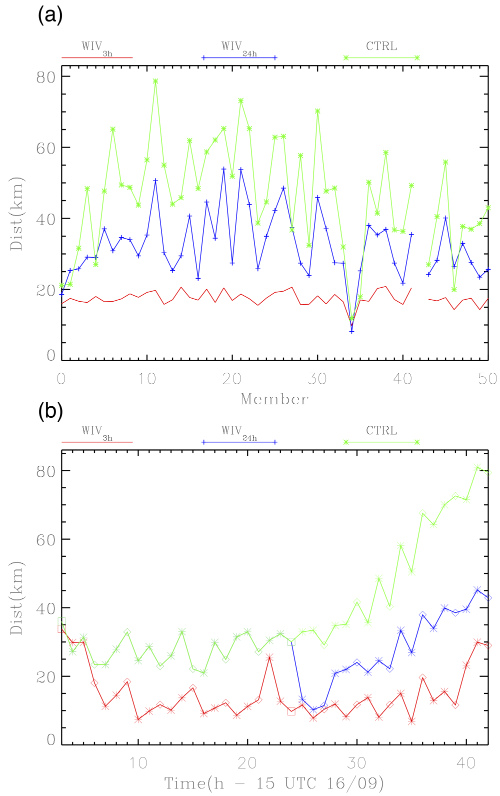

Figure 8. Average error of the ensembles $CTRL$, WIV_{24h}, and WIV_{3h} as function of a) the member; and, b) the time. In the panel b), diamonds are shown every 3h while the square is every 24h from the simulation start.

To study the impact of WIVERN DA on the forecast in more detail, we focus on the member 10, one of the members showing a substantial impact of WIVERN DA. Figure 9 shows the application of the 3DVar to this member; the background (panel a) represents the strong winds associated with the Medicane Ianos, with meridional wind speeds reaching up to about 40 ms^{-1}, and a cyclonic circulation around the storm center (bipolar structure). After assimilation (panel b), the winds are still very intense and the cyclonic circulation well represented; however, the whole circulation has shifted several tens of kilometers to the east (refer to the longitude $17.5°E$).

The difference between the two fields has a "tripolar" pattern (panel c). From west to east, the meridional wind difference is positive to the west of $17.5°E$, negative between $17.5°E$ and $19°E$, and then positive again towards the east. This pattern corresponds to the net eastward shift of the storm center, and to a small reinforcement of the meridional wind component. The vertical cross-section of the zonal wind difference (analysis minus background) is shown in Figure 9 panel d). It highlights a main dipolar pattern close to the storm center (around $38.5°N$), with negative values reaching up to 20 ms^{-1} at about 2500 m a.s.l. This dipolar pattern reaches up to 6 km height and is a consequence of the eastward shift of the storm center in the analysis.

In the upper troposphere, the difference between the analysis and background becomes more complex with several localized positive and negative values. This pattern is determined by observations at these levels and by the vertical structure of the background error matrix. Smaller differences are seen further north; they are caused by pseudo-observations over the NE of the domain.

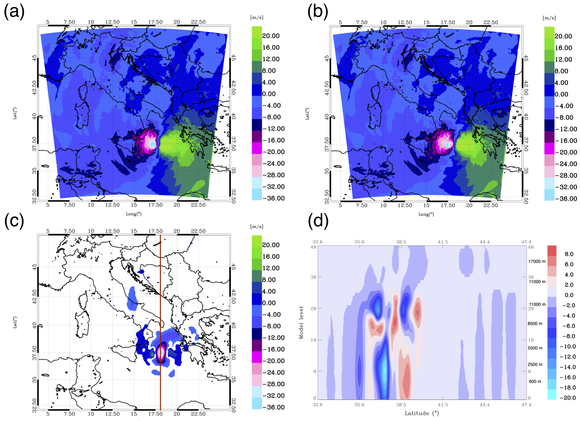

Figure 9. Analysis of wind components at 12 UTC on 17 September 2020 for member 10: a) background meridional wind component at about 2500 m a.s.l; b) analysis of the meridional wind component at about 2500 m a.s.l; c) difference between analysis and background fields of the meridional wind component (same level of panels a-b); d) cross-section of the difference between the analysis and the background of the zonal wind component along the red line of panel c). The y-axis of panel d) shows the vertical levels and labels on the right y-axis correspond to the approximate height of the levels.

The 18 h forecast of the sea level pressure and surface winds starting from the analysis of Figure 9 is shown in Figure 10. The impact of WIVERN DA on the evolution of this member is very high. First, the position of the storm is much improved by WIVERN DA; while the member 42 (panel a) has just crossed the Zakynthos island, the storm center of member 10 without WIVERN DA is in the open sea (about 100 km to the SW of Zakynthos). The storm center of the member 10 after DA is close (about 10 km kilometers) to Zakynthos. Importantly, the minimum sea level pressure is also adjusted with WIVERN DA; it is about 983 hPa for member 42 and for member 10 after DA, while it is lower than 975 hPa for member 10 without data assimilation. Similarly, the maximum wind speed at the surface of member 10 with WIVERN DA (28.1 ms^{-1}) is much closer to the representative member 42 (31 ms^{-1}) compared to the member 10 without WIVERN DA (39.8 ms^{-1}). In summary, Figure 10 shows that the assimilation of WIVERN winds changes the evolution of the storm not only for the trajectory but also for the physical characteristics, providing a more realistic representation of the Medicane Ianos.

3.1 Impacts on the precipitation and surface winds forecasts

In this section we discuss the impact of assimilating the WIVERN winds along the LoS on the prediction of the precipitation and surface winds. Figure 11 shows the precipitation accumulated from 12 UTC on 17 September to 12 UTC on 18 September

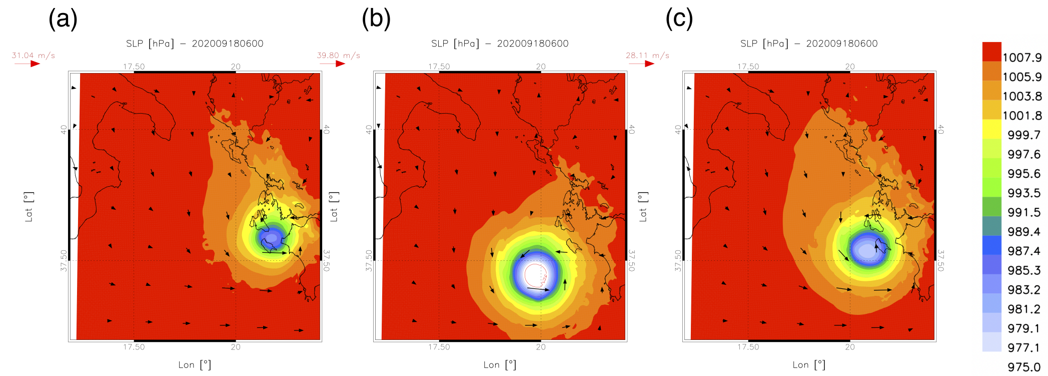

Figure 10. Sea level pressure and surface winds (every 20 grid points) at 06 UTC on 18 September for a) member 42; b) member 10, c) member 10 after the assimilation of WIVERN winds at 12 UTC on 17 September. The panels refer at 06 UTC on 18 September, i.e. 18 h after the assimilation time. The contour inside the Medicane eye in panel b) corresponds to the 975 hPa isobar.

for the $CTRL$ ensemble (average), the representative member 42, and the WIV_{24h} ensemble (average). The precipitation accumulated by the member 42 clearly mirrors the trajectory followed by the cyclone with accumulated rainfall larger than 300 mm day^{-1} in a swath oriented from SW to NE, ending over the Kefalonia island.

The $CTRL$ ensemble shows a precipitation pattern which is oriented in the NW-SE direction, differently from the pattern of the member 42. The field of $CTRL$ is smoothed compared to the representative member, but this feature is caused by the average operator. The precipitation on the island of Kefalonia is largely underestimated because the rainfall is 150 mm day^{-1} for $CTRL$ compared to more than 300 mm day^{-1} of the forecast for the member 42.

The rainfall accumulated by the ensemble WIV_{24h} is in better agreement with the representative member 42 compared to $CTRL$ because the intense precipitation swath is better oriented in the SW-NE direction and the rainfall predicted over Kefalonia is greater than 300 mm day^{-1}. The better forecast of the WIV_{24h} compared to $CTRL$ is confirmed by the RMSE, calculated respect to member 42 and averaged over the area defined by the longitudes 17.5-22.5^{o}E and by the latitudes 36.0-39.0$°N$ (red rectangle of Figure 11, panel c), which decreases from 51.0 mm of $CTRL$ to 40.5 mm of WIV_{24h}.

Figure 12 shows the errors of the ensembles $CTRL$ and WIV_{24h} calculated with respect to the member 42 for the surface winds for the coordinates corresponding to the island of Kefalonia (20.7$°E$; 38.15$°N$) at 06 UTC on 18 September. The time is that of Figure 10 and the surface wind simulated by the member 42 in correspondence of the selected position is from NE with an intensity of 26 ms^{-1}. The members of both ensembles are underestimating the wind intensity in Kefalonia. However, the underestimation is greater for the $CTRL$ ensemble compared to WIV_{24h}, as shown by the error distributions of Figure 12 panel a), which is more skewed towards negative values for the $CTRL$ ensemble. For example, 26 members of the $CTRL$ ensemble underestimate the wind intensity by more than 14 ms^{-1}, while this number is reduced to 4 for the WIV_{24h} ensemble. The statistics for the whole ensemble are shown in Table 2.

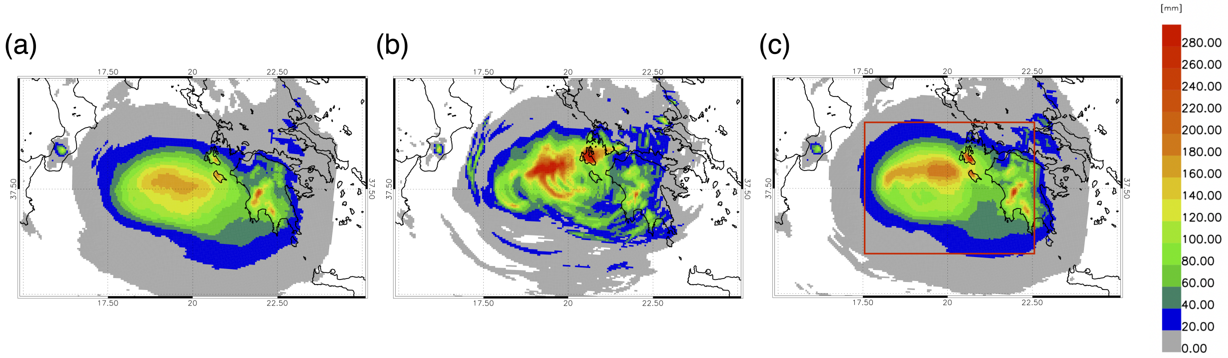

Figure 11. Rainfall accumulated from the 12 UTC on 17 September to 12 UTC on 18 September by: a) the $CTRL$ ensemble (average); b) the representative member 42; c) the WIV_{24h} ensemble (average).

Table 2. Wind speed Bias and RMSE computed for the Kefalonia site (20.7° E; 38.15° N) for the ensemble $CTRL$ and WIV_{24h}. WIV_{3h} is also reported for completeness

EXP	Bias [m/s]	RMSE [m/s]
$CTRL$	-10.7	12.3
WIV_{3h}	-5.3	6.2
WIV_{24h}	-6.3	7.7

Even if less apparent, similar considerations apply to the wind direction, shown in Figure 12 panel b). The $CTRL$ ensemble has more members with errors larger than 75 ° compared to WIV_{24h}. The Bias of the direction is positive and winds are coming more from E-SE in the $CTRL$ and WIV_{24h} ensembles compared to member 42. This is coherent with simulating the storm center to the southwest of the member 42.

3.2 Sensitivity to model and observations error

In this section we consider the results of two sensitivity tests: in the first test we inflated the observation error, in the second test we changed the background error matrix. For the first experiment the observation error is assumed to be equal to the model error and dependent only on height. The observation error is shown in Figure 4 (panel b, curve $E2$) and corresponds to the situation in which the analysis gives an equal weight to the background and to the observations. Considering the error of Figure 4 this sensitivity test roughly corresponds to inflating the WIVERN error by a factor of 2 and we will refer to this experiment as $E2$.

In the second sensitivity experiment, we changed the background error matrix, which was computed applying the NMC (Parrish and Derber, 1992) method to the period 1 September 2020 - 30 September 2020. Specifically, the background error matrix was

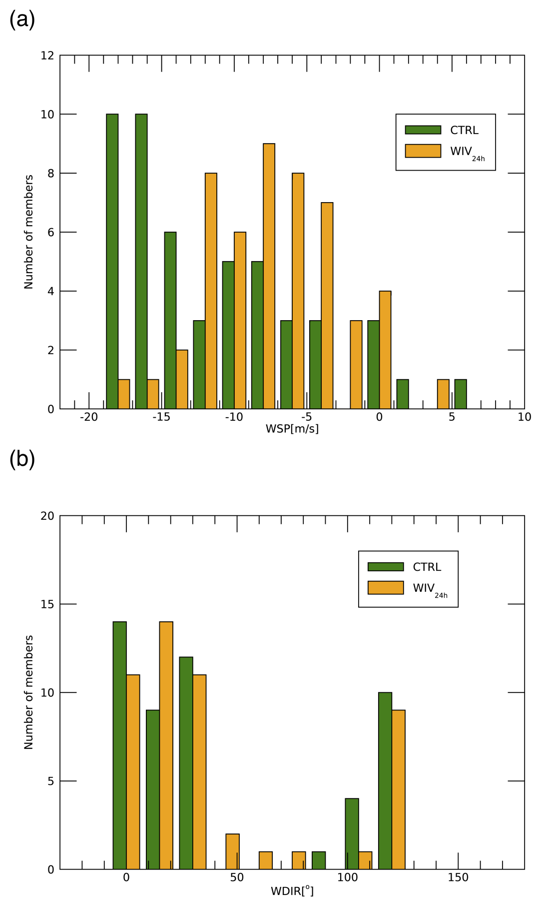

Figure 12. Distribution of the errors of the ensemble members for the surface winds at Kefalonia for $CTRL$ and WIV_{24h}. Errors are computed compared to member 42 at the 06 UTC on 18 September for a) wind speed; b) wind direction. The histogram bins are 2.0 ms^{-1} for the wind speed and 15 $^{\circ}$ for the direction.

Table 3. Wind direction Bias and RMSE computed for the Kefalonia site (20.7° E; 38.15° N) for the ensemble $CTRL$ and WIV_{24h}.

EXP	Bias [°]	RMSE[°]
$CTRL$	51.7	71.0
WIV_{3h}	20.2	23.9
WIV_{24h}	45.1	62.0

computed from the difference of two forecasts verifying at the same time (both 12 UTC and 00 UTC) for the whole period. The background error matrix was computed using the operational analysis/forecast cycle issued by the ECMWF at 00 UTC and 12 UTC as initial and boundary conditions of the WRF model. In this configuration the background error matrix is representative of the meteorological conditions of the month of September 2020, while in the approach used for the WIV_{24h} experiment, Eqn. (1), the background error matrix is representative of the error of the day. This sensitivity experiment will be referred to as NMC.

Results of both experiments are represented by the distribution of the trajectory errors of the ensemble members, shown in Figure 13. The largest error correspond to the $CTRL$ experiment, followed by NMC, $E2$, and WIV_{24h} experiments. The assimilation of WIVERN winds has, in general, a positive impact on the prediction of the Medicane Ianos trajectory as the experiment with doubled observation error has a performance much closer to WIV_{24h} than to $CTRL$. Specifically, the average error of the experiment $E2$ is 34.4 km, very similar to that of WIV_{24h} ensemble, however the median error is larger (35.4 km) for $E2$ compared to WIV_{24h} (32.7 km). Similarly, the spread of the ensemble error is larger for $E2$ (14.5 km) compared to WIV_{24h} (13.3 km). Statistics for the trajectories error distributions are summarized in Table 4.

To better understand the low sensitivity of this case study to the observation error, Figure 14, shows the BIAS, MAE and RMSE

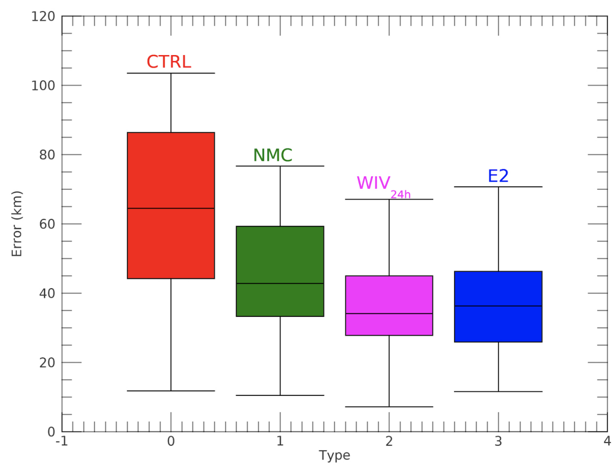

Figure 13. Trajectories error distribution, respect to the representative member 42, of the ensembles $CTRL$, NMC, WIV_{24h} and $E2$. The boxes show the 25^{th} and the 75^{th} percentile, the black line inside the box is the median and the maximum and minimum values are the extremes of the error bar.

for the first guess as a function of the vertical level. The first guess error (RMSE) is larger than the observation error and also of the model error (Figure 4, panel b), and inflating the observation error has a relatively small impact on the WIVERN winds DA performance. However, it is important to point out that winds around Medicanes are very intense, and a wrong positioning of the storm results in high first-guess errors for the winds; in general it is expected that the role of the WIVERN observation error is larger than that reported for the Ianos case study.

Changing the background error matrix for this specific case has a notable impact on the trajectory forecast. This is expected in some measure, as the physical characteristics of the Medicane is rather different from those of the circulation of the period. Specifically, the trajectory error averaged over the whole ensemble for the NMC experiment is 44.7 km (35.4 km for

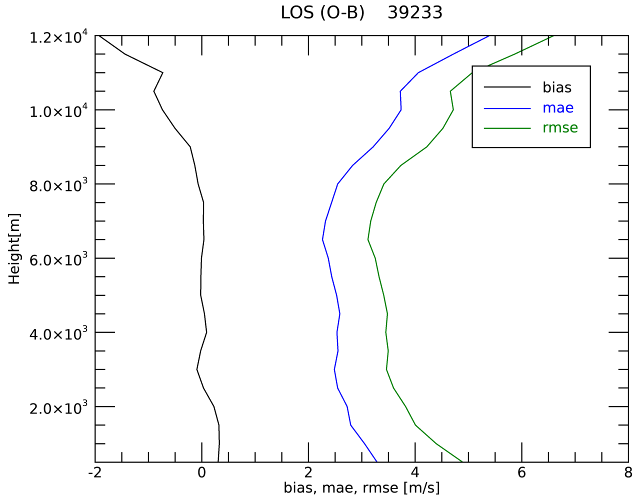

Figure 14. Observation minus background errors [m/s] for the winds along the line of sight as a function of the vertical levels.

WIV_{24h}), the median is 42.7 km (32.7 km for WIV_{24h}) and the spread of the ensemble is 16.9 km (13.3 km for WIV_{24h}). All these statistics show the sensitivity of the WIVERN DA impact to the choice of the background error matrix (Table 4).

Table 4. Statistics of the trajectories error distribution, respect to the representative member 42, of the ensembles $CTRL$, NMC, WIV_{24h} and $E2$.

EXP	Mean [km]	Median [km]	Spread [km]
$CTRL$	62.5	64.4	24.2
NMC	44.7	42.7	16.9
WIV_{24h}	34.4	32.7	13.3
$E2$	34.4	35.4	14.5

4 Conclusions

In this paper we considered the assimilation of WIVERN winds along the Line of Sight (LoS) in the WRF model for the case study of the Medicane Ianos. The assimilation is done in an ensemble context and pseudo-observations are generated from one member of the ensemble whose trajectory is in best agreement with the best estimated trajectory of Ianos.

Two 3DVar assimilation cycles are considered: 3 h and 24 h. The first case, with very frequent data assimilation cycles, is used to verify the proper setting of the 3DVar and WRF model; it could represent a realistic condition if a constellation of many (4) WIVERN satellites were operated. The second case corresponds to the realistic situation in which WIVERN samples the Ianos storm once.

Results shows an important impact of WIVERN wind DA on the WRF forecast. Considering the trajectory forecast, the average error is improved by more than 40% and the error decreases from 62.5 km to 35.4 km. It is shown that the trajectory forecast is improved for 46 out of 50 members and that this improvement lasts at least 18 h. The forecast improvement is not confined to the trajectories but it is transferred from the dynamic to the mass field through the model physics, as shown by the improvement of the sea level pressure forecast and surface wind speed. This consideration applies also to the rainfall forecast which, with WIVERN DA, is more in agreement with that of the representative member for both pattern and intensity.

Finally, we presented the results of two sensitivity tests changing the observation and background errors. For the specific case of the Medicane Ianos, the impact of changing the background error matrix has a larger impact. This is caused by two main reasons: a) the first guess error is larger than the background and observation errors, also when the latter is inflated and the impact of assimilating WIVERN is expected high; b) as Medicanes are storms with peculiar characteristics, the background error matrix derived from the ensemble and representative of the "error of the day" is more appropriate for DA than the background error matrix computed for the whole period.

Recently, Pantillon et al. (2024) published a paper showing a model intercomparison for the Medicane Ianos forecast with 10 models participating to the comparison (including WRF). One of the aspects considered in the paper is the simulation of the Ianos trajectory from different models. Results show a spread of the models trajectories which is in line with the results shown by the $CTRL$ ensemble; in addition most of the trajectories go to the south of the best estimated trajectory followed by Ianos, in agreement with the results of the $CTRL$ ensemble. In this sense, the results of this paper show that the WIVERN winds DA has the potential to narrow down the spread among different models in the forecast of such events.

While the performance of WIVERN DA for the Ianos case study is promising there are few points that limit the results of this work. First, we considered only one case study and no general conclusions can be derived on the performance of the WIVERN DA at the regional scale. Second, we assimilated WIVERN only data, neglecting the global observing system, which is, however, considered indirectly from the ECMWF initialisation. This could result in an overestimation of the WIVERN impact in the forecast of the Medicane Ianos. Studies are in progress considering this point, and preliminary results show an important impact of WIVERN winds DA compared to other data sources. Third we assumed that the storm is well sampled and that the Medicane is nearly at the center of the satellite swath. Considering the above limitations of this study, the results shown in this paper could represent an upper limit of what expected from the DA of WIVERN winds at the regional scale and further studies are needed to precisely quantify this point.

Code and data availability. The 3DVar software with the latest updates can be downloaded from the webpage meteo.artov.isac.cnr.it . Data can be requested to the corresponding author.

Appendix A: Assimilation of WIVERN Doppler by 3DVar

This Appendix provides further details about the 3DVar. We use the incremental formulation of the cost-function; let's $\boldsymbol{x}$ denote the state vector and $\delta\boldsymbol{x} = \boldsymbol{x} - \boldsymbol{x}^b$ the increment respect to the background state vector $\boldsymbol{x}^b$, the 3DVar cost-function is:

$$J(\boldsymbol{x}) = \underbrace{\frac{1}{2}\delta\boldsymbol{x}^T\mathbf{B}^{-1}\delta\boldsymbol{x}}_{J^b} + \underbrace{\frac{1}{2}(\mathbf{H}\delta\boldsymbol{x} - \boldsymbol{d})^T\mathbf{R}^{-1}(\mathbf{H}\delta\boldsymbol{x} - \boldsymbol{d})}_{J^o} \tag{A1}$$

where $\mathbf{B}$ is the background error matrix, $\mathbf{R}$ is the observations error matrix, $\boldsymbol{d} = \boldsymbol{y_o} - H(\boldsymbol{x^b})$ are the innovations and H is the forward observation operator, transforming the state vector into the observation space, and $\mathbf{H}$ is the derivative of H respect to $\boldsymbol{x}$. The $\mathbf{B^{-1}}$, due to its large dimensions, cannot be calculated directly with inversion matrix techniques and we introduce a pre-conditioning transform $\mathbf{U}$ such that $\mathbf{B} = \mathbf{U}\mathbf{U}^T$. With this transform the analysis control variable is $\boldsymbol{\nu}$, where $\delta\boldsymbol{x} = \mathbf{U}\boldsymbol{\nu}$, and $2J^b = \boldsymbol{\nu}^T\boldsymbol{\nu}$. The cost-function becomes:

$$J(\boldsymbol{\nu}) = \underbrace{\frac{1}{2}\boldsymbol{\nu}^T\boldsymbol{\nu}}_{J^b} + \underbrace{\frac{1}{2}(\mathbf{H}\mathbf{U}\boldsymbol{\nu} - \boldsymbol{d})^T\mathbf{R}^{-1}(\mathbf{H}\mathbf{U}\boldsymbol{\nu} - \boldsymbol{d})}_{J^o} \tag{A2}$$

The transformation $\mathbf{U}$ is given by a series of simpler transform in the x, y and z directions, and the order of their application is important. In the 3DVar used in this work $\mathbf{U} = \mathbf{U_z}\mathbf{U_y}\mathbf{U_x}$, where $\mathbf{U_x}$, $\mathbf{U_y}$ and $\mathbf{U_z}$ are computed starting form the background error matrices in the x, y and z directions using eigenvalue-eigenvector decompositions. Specifically, $\mathbf{B_x}$ and $\mathbf{B_y}$ are specified as correlation error matrices whose length-scales are computed from the NMC (National Meteorological Center) method (see Barker et al. (2004) for details), while $\mathbf{U_z}$ is calculated by the eigenvalue-eigenvector decomposition of the vertical background error matrix (see Federico (2013) for details). In the 3DVar formulation of this paper, the length-scales in the x and y directions are equal to each other and are functions of the vertical level. The length-scales are around 20-30 km from the surface up to 5 km height, then they increases from 30 km to 50-60 km in the height range 6000 m-11000 m, then the length-scales decrease again in the upper troposphere and lower stratosphere and are in the range 20-40 km for heights above 15000 m.

Figure A1 shows the simplest example of assimilating one WIVERN observation Y_o for a one-dimensional grid formed by two grid-points (1 and 2) with wind components (U_1, V_1) and (U_2, V_2), respectively. Denoting ξ the fraction distance of the observation from the grid-point 1, the vector $H(\boldsymbol{x^b})$ and the operator $\mathbf{H}$ are given by:

$$H(\boldsymbol{x^b}) = \begin{pmatrix} (1-\xi)\cos\phi\sin\theta \\ \xi\cos\phi\sin\theta \\ (1-\xi)\sin\phi\sin\theta \\ \xi\sin\phi\sin\theta \end{pmatrix}^T \begin{pmatrix} U_1 \\ V_1 \\ U_2 \\ V_2 \end{pmatrix} \tag{A3}$$

and:

$$\mathbf{H} = \begin{pmatrix} (1-\xi)\cos\phi\sin\theta \\ \xi\cos\phi\sin\theta \\ (1-\xi)\sin\phi\sin\theta \\ \xi\sin\phi\sin\theta \end{pmatrix}^T \tag{A4}$$

Finally, the minimization of the cost-function J is done iteratively with the conjugate gradient method by calculation of the gradient $\nabla_\nu J$:

$$\nabla_\nu J = \nu + U^T H^T R^{-1}(\mathbf{H}\mathbf{U}\boldsymbol{\nu} - \boldsymbol{d}) \tag{A5}$$

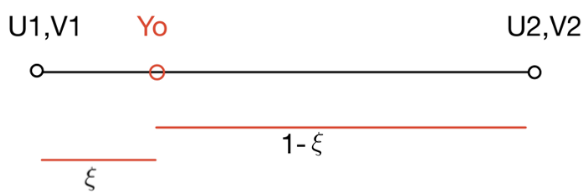

Figure A1. The simplest example of an observation, Y_o, between two grid-points.

Author contributions. SF and MM coordinated the experiment; SF, RCT and CT maintain and develop the 3DVar code, SF provided the simulations; AB provided the WIVERN simulator; AB and MP provided feedback and information on WIVERN; SF prepared the paper and the figures. All authors discussed and provided feedback on the manuscript.

Competing interests. The authors declare that no competing interests are present.

Acknowledgements. The work by C. Cambiotti and A. Battaglia has been funded by the Italian Space Agency (ASI) project “Scientific studies for the Wind Velociy Radar Nephoscope (WIVERN) mission” (Project number: 2023-44-HH.0). The work by F. Manconi was carried out within the Space It Up project funded by the Italian Space Agency, ASI, and the Ministry of University and Research, MUR, under contract n. 2024-5-E.0 - CUP n. I53D24000060005.

References

Ali, E., Cramer, W., Carnicer, J., Georgopoulou, E., Hilmi, N., Le Cozannet, G., and Lionello, P.: Climate Change 2022 – Impacts, Adaptation and Vulnerability: Working Group II Contribution to the Sixth Assessment Report of the Intergovernmental Panel on Climate Change. Mediterranean Region., p. 2233–2272, Cambridge University Press, 2023.

Androulidakis, Y., Makris, C., Mallios, Z., Pytharoulis, I., Baltikas, V., and Krestenitis, Y.: Storm surges and coastal inundation during extreme events in the Mediterranean Sea: the IANOS Medicane, Natural Hazards, 117, 939–978, https://doi.org/10.1007/s11069-023-05890-6, 2023.

Baker, W. E., Atlas, R., Cardinali, C., Clement, A., Emmitt, G. D., Gentry, B. M., Hardesty, R. M., Källén, E., Kavaya, M. J., Langland, R., Ma, Z., Masutani, M., McCarty, W., Pierce, R. B., Pu, Z., Riishojgaard, L. P., Ryan, J., Tucker, S., Weissmann, M., and Yoe, J. G.: Lidar-Measured Wind Profiles: The Missing Link in the Global Observing System:, Bulletin of the American Meteorological Society, 95, 543 – 564, https://doi.org/10.1175/BAMS-D-12-00164.1, 2014.

Barker, D. M., Huang, W., Guo, Y.-R., Bourgeois, A. J., and Xiao, Q. N.: A Three-Dimensional Variational Data Assimilation System for MM5: Implementation and Initial Results, Monthly Weather Review, 132, 897 – 914, https://doi.org/10.1175/1520-0493(2004)132<0897:ATVDAS>2.0.CO;2, 2004.

Battaglia, A., Martire, P., Caubet, E., Phalippou, L., Stesina, F., Kollias, P., and Illingworth, A.: Observation error analysis for the WInd VElocity Radar Nephoscope W-band Doppler conically scanning spaceborne radar via end-to-end simulations, Atmospheric Measurement Techniques, 15, 3011–3030, https://doi.org/10.5194/amt-15-3011-2022, 2022.

Battaglia, A., Rabino, R., Mroz, K., Tridon, F., and Parodi, A.: Non uniform beam filling correction for the Doppler velocity measured by the WIVERN conically scanning radar, J. Atmos. Ocean. Technol., submitted, 2025a.

Battaglia, A., Rizik, A., Sikaneta, I., and Tridon, F.: I and Qs Simulation and Processing Envisaged for Spaceborne Polarization Diversity Doppler Radars, 63, 1–14, https://doi.org/10.1109/TGRS.2025.3529672, 2025b.

Comellas Prat, A., Federico, S., Torcasio, R. C., D'Adderio, L. P., Dietrich, S., and Panegrossi, G.: Evaluation of the Sensitivity of Medicane Ianos to Model Microphysics and Initial Conditions Using Satellite Measurements, Remote Sensing, 13, https://doi.org/10.3390/rs13244984, 2021.

Da Silva, S. L. E., Battaglia, A., Cambiotti, C., and Carbone, A. F.: Reconstruction of the horizontal wind field inside weather systems from the sparse sampling envisaged for the WIVERN mission, IEEE Transactions on Geoscience and Remote Sensing, submitted, 2025.

D'Adderio, L. P., Casella, D., Dietrich, S., Sanò, P., and Panegrossi, G.: GPM-CO observations of Medicane Ianos: Comparative analysis of precipitation structure between development and mature phase, Atmospheric Research, 273, 106 174, https://doi.org/https://doi.org/10.1016/j.atmosres.2022.106174, 2022.

Dafis, S., Claud, C., Kotroni, V., Lagouvardos, K., and Rysman, J.-F.: Insights into the convective evolution of Mediterranean tropical-like cyclones, Quarterly Journal of the Royal Meteorological Society, 146, 4147–4169, https://doi.org/https://doi.org/10.1002/qj.3896, 2020.

Di Francesca, V., D'Adderio, L. P., Sanò, P., Rysman, J.-F., Casella, D., and Panegrossi, G.: Passive microwave-based diagnostics of medicanes over the period 2000–2021, Atmospheric Research, 316, 107 922, https://doi.org/https://doi.org/10.1016/j.atmosres.2025.107922, 2025.

Dudhia, J.: Numerical Study of Convection Observed during the Winter Monsoon Experiment Using a Mesoscale Two-Dimensional Model, Journal of Atmospheric Sciences, 46, 3077–3107, https://doi.org/https://doi.org/10.1175/1520-0469(1989)046<3077:NSOCOD>2.0.CO;2, 1989.

Emanuel, K.: Genesis and maintenance of "Mediterranean hurricanes", Advances in Geosciences, 2, 217–220, https://doi.org/10.5194/adgeo-2-217-2005, 2005.

Federico, S.: Implementation of a 3D-Var system for atmospheric profiling data assimilation into the RAMS model: initial results, Atmospheric Measurement Techniques, 6, 3563–3576, https://doi.org/10.5194/amt-6-3563-2013, 2013.

Feng, C. and Pu, Z.: The impacts of assimilating Aeolus horizontal line-of-sight winds on numerical predictions of Hurricane Ida (2021) and a mesoscale convective system over the Atlantic Ocean, Atmospheric Measurement Techniques, 16, 2691–2708, https://doi.org/10.5194/amt-16-2691-2023, 2023.

Ferrarin, C., Pantillon, F., Davolio, S., Bajo, M., Miglietta, M. M., Avolio, E., Carrió, D. S., Pytharoulis, I., Sanchez, C., Patlakas, P., González-Alemán, J. J., and Flaounas, E.: Assessing the coastal hazard of Medicane Ianos through ensemble modelling, Natural Hazards and Earth System Sciences, 23, 2273–2287, https://doi.org/10.5194/nhess-23-2273-2023, 2023.

Fita, L. and Flaounas, E.: Medicanes as subtropical cyclones: the December 2005 case from the perspective of surface pressure tendency diagnostics and atmospheric water budget, Quarterly Journal of the Royal Meteorological Society, 144, 1028–1044, https://doi.org/https://doi.org/10.1002/qj.3273, 2018.

Flaounas, E., Gray, S. L., and Teubler, F.: A process-based anatomy of Mediterranean cyclones: from baroclinic lows to tropical-like systems, Weather and Climate Dynamics, 2, 255–279, https://doi.org/10.5194/wcd-2-255-2021, 2021.

Flaounas, E., Davolio, S., Raveh-Rubin, S., Pantillon, F., Miglietta, M. M., Gaertner, M. A., Hatzaki, M., Homar, V., Khodayar, S., Korres, G., Kotroni, V., Kushta, J., Reale, M., and Ricard, D.: Mediterranean cyclones: current knowledge and open questions on dynamics, prediction, climatology and impacts, Weather and Climate Dynamics, 3, 173–208, https://doi.org/10.5194/wcd-3-173-2022, 2022.

Flaounas, E., Aragão, L., Bernini, L., Dafis, S., Doiteau, B., Flocas, H., Gray, S. L., Karwat, A., Kouroutzoglou, J., Lionello, P., Miglietta, M. M., Pantillon, F., Pasquero, C., Patlakas, P., Picornell, M. A., Porcù, F., Priestley, M. D. K., Reale, M., Roberts, M. J., Saaroni, H., Sandler, D., Scoccimarro, E., Sprenger, M., and Ziv, B.: A composite approach to produce reference datasets for extratropical cyclone tracks: application to Mediterranean cyclones, Weather and Climate Dynamics, 4, 639–661, https://doi.org/10.5194/wcd-4-639-2023, 2023.

Garrett, K., Liu, H., Ide, K., Hoffman, R. N., and Lukens, K. E.: Optimization and impact assessment of Aeolus HLOS wind assimilation in NOAA's global forecast system, Quarterly Journal of the Royal Meteorological Society, 148, 2703–2716, https://doi.org/https://doi.org/10.1002/qj.4331, 2022.

Hagelin, S., Azad, R., Lindskog, M., Schyberg, H., and Körnich, H.: Evaluating the use of Aeolus satellite observations in the regional numerical weather prediction (NWP) model Harmonie–Arome, Atmospheric Measurement Techniques, 14, 5925–5938, https://doi.org/10.5194/amt-14-5925-2021, 2021.

Harnisch, F., Healy, S. B., Bauer, P., and English, S. J.: Scaling of GNSS Radio Occultation Impact with Observation Number Using an Ensemble of Data Assimilations, Monthly Weather Review, 141, 4395 – 4413, https://doi.org/10.1175/MWR-D-13-00098.1, 2013.

Horányi, A., Cardinali, C., Rennie, M., and Isaksen, L.: The assimilation of horizontal line-of-sight wind information into the ECMWF data assimilation and forecasting system. Part I: The assessment of wind impact, Quarterly Journal of the Royal Meteorological Society, 141, 1223–1232, https://doi.org/https://doi.org/10.1002/qj.2430, 2015.

Illingworth, A. J., Battaglia, A., Bradford, J., Forsythe, M., Joe, P., Kollias, P., Lean, K., Lori, M., Mahfouf, J.-F., Melo, S., Midthassel, R., Munro, Y., Nicol, J., Potthast, R., Rennie, M., Stein, T. H. M., Tanelli, S., Tridon, F., Walden, C. J., and Wolde, M.: WIVERN: A New Satellite Concept to Provide Global In-Cloud Winds, Precipitation, and Cloud Properties, Bulletin of the American Meteorological Society, 99, 1669–1687, https://doi.org/10.1175/BAMS-D-16-0047.1, 2018.

Janjic, Z. I.: The Step-Mountain Eta Coordinate Model: Further Developments of the Convection, Viscous Sublayer, and Turbulence Closure Schemes, Monthly Weather Review, 122, 927–945, https://doi.org/10.1175/1520, 1994.

Lagouvardos, K., Karagiannidis, A., Dafis, S., Kalimeris, A., and Kotroni, V.: Ianos—A Hurricane in the Mediterranean, Bulletin of the American Meteorological Society, 103, E1621 – E1636, https://doi.org/https://doi.org/10.1175/BAMS-D-20-0274.1, 2022.

Lfarh, W., Pantillon, F., and Chaboureau, J.-P.: The Downward Transport of Strong Wind by Convective Rolls in a Mediterranean Windstorm, Monthly Weather Review, 151, 2801 – 2817, https://doi.org/10.1175/MWR-D-23-0099.1, 2023.

Li, L., Žagar, N., Raeder, K., and Anderson, J. L.: Comparison of temperature and wind observations in the Tropics in a perfect-model, global EnKF data assimilation system, Quarterly Journal of the Royal Meteorological Society, 149, 2367–2385, https://doi.org/https://doi.org/10.1002/qj.4511, 2023.

Martin, A., Weissmann, M., and Cress, A.: Investigation of links between dynamical scenarios and particularly high impact of Aeolus on numerical weather prediction (NWP) forecasts, Weather and Climate Dynamics, 4, 249–264, https://doi.org/10.5194/wcd-4-249-2023, 2023.

Matsangouras, I., Avgoustoglou, E., Pytharoulis, I., and Nastos, P.: The Impact of Aeolus Wind Profile Measurements on Severe Weather Events: A COSMO NWP Case Study over Thessaly, Environmental Sciences Proceedings, 26, https://doi.org/10.3390/environsciproc2023026047, 2023.

Miglietta, M. M. and Rotunno, R.: Development mechanisms for Mediterranean tropical-like cyclones (medicanes), Quarterly Journal of the Royal Meteorological Society, 145, 1444–1460, https://doi.org/https://doi.org/10.1002/qj.3503, 2019.

Mlawer, E. J., Taubman, S. J., Brown, P. D., Iacono, M. J., and Clough, S. A.: Radiative transfer for inhomogeneous atmospheres: RRTM, a validated correlated-k model for the longwave, Journal of Geophysical Research: Atmospheres, 102, 16 663–16 682, https://doi.org/https://doi.org/10.1029/97JD00237, 1997.

Pantillon, F., Davolio, S., Avolio, E., Calvo-Sancho, C., Carrió, D. S., Dafis, S., Gentile, E. S., Gonzalez-Aleman, J. J., Gray, S., Miglietta, M. M., Patlakas, P., Pytharoulis, I., Ricard, D., Ricchi, A., Sanchez, C., and Flaounas, E.: The crucial representation of deep convection for the cyclogenesis of Medicane Ianos, Weather and Climate Dynamics, 5, 1187–1205, https://doi.org/10.5194/wcd-5-1187-2024, 2024.

Parrish, D. F. and Derber, J. C.: The National Meteorological Center's Spectral Statistical-Interpolation Analysis System, Monthly Weather Review, 120, 1747 – 1763, https://doi.org/10.1175/1520-0493(1992)120<1747:TNMCSS>2.0.CO;2, 1992.

Rani, S. I., Jangid, B. P., Kumar, S., Bushair, M. T., Sharma, P., George, J. P., George, G., and Das Gupta, M.: Assessing the quality of novel Aeolus winds for NWP applications at NCMRWF, Quarterly Journal of the Royal Meteorological Society, 148, 1344–1367, https://doi.org/https://doi.org/10.1002/qj.4264, 2022.

Raveh-Rubin, S. and Wernli, H.: Large-scale wind and precipitation extremes in the Mediterranean: dynamical aspects of five selected cyclone events, Quarterly Journal of the Royal Meteorological Society, 142, 3097–3114, https://doi.org/https://doi.org/10.1002/qj.2891, 2016.

Rennie, M. P., Isaksen, L., Weiler, F., de Kloe, J., Kanitz, T., and Reitebuch, O.: The impact of Aeolus wind retrievals on ECMWF global weather forecasts, Quarterly Journal of the Royal Meteorological Society, 147, 3555–3586, https://doi.org/https://doi.org/10.1002/qj.4142, 2021.

Sanchez, C., Gray, S., Volonte, A., Pantillon, F., Berthou, S., and Davolio, S.: How a warmer Mediterranean preconditions the upper-level environment for the development of Medicane Ianos, EGUsphere, 2023, 1–35, https://doi.org/10.5194/egusphere-2023-2431, 2023.

Saraceni, M., Silvestri, L., Bechtold, P., and Bongioannini Cerlini, P.: Mediterranean tropical-like cyclone forecasts and analysis using the ECMWF ensemble forecasting system with physical parameterization perturbations, Atmospheric Chemistry and Physics, 23, 13 883–13 909, https://doi.org/10.5194/acp-23-13883-2023, 2023.

Scarsi, F. E., Battaglia, A., Maahn, M., and Lhermitte, S.: How to reduce sampling errors in spaceborne cloud radar-based snowfall estimates, EGUsphere, 2024, 1–23, https://doi.org/10.5194/egusphere-2024-1917, 2024a.

Scarsi, F. E., Battaglia, A., Tridon, F., Martire, P., Dhillon, R., and Illingworth, A.: Mispointing characterization and Doppler velocity correction for the conically scanning WIVERN Doppler radar, 17, 499–514, https://doi.org/10.5194/amt-17-499-2024, 2024b.

Skamarock, W., Klemp, J., Dudhia, J., Gill, D., Liu, Z., Berner, J., Wang, W., Powers, J., Duda, M., Barker, D., and Huang, X.-Y.: A Description of the Advanced Research WRF, Version 4, https://doi.org/10.5065/1dfh-6p97, 2019.

Stathopoulos, C., Chaniotis, I., and Patlakas, P.: Assimilating Aeolus Satellite Wind Data on a Regional Level: Application in a Mediterranean Cyclone Using the WRF Model, Atmosphere, 14, https://doi.org/10.3390/atmos14121811, 2023.

Tan, D. G. H., Andersson, E., Fisher, M., and Isaksen, L.: Observing-system impact assessment using a data assimilation ensemble technique: application to the ADM–Aeolus wind profiling mission, Quarterly Journal of the Royal Meteorological Society, 133, 381–390, https://doi.org/https://doi.org/10.1002/qj.43, 2007.

Thompson, G., Field, P. R., Rasmussen, R. M., and Hall, W. D.: Explicit Forecasts of Winter Precipitation Using an Improved Bulk Microphysics Scheme. Part II: Implementation of a New Snow Parameterization, Monthly Weather Review, 136, 5095 – 5115, https://doi.org/https://doi.org/10.1175/2008MWR2387.1, 2008.

Torcasio, R. C., Papa, M., Del Frate, F., Mascitelli, A., Dietrich, S., Panegrossi, G., and Federico, S.: Data Assimilation of Satellite-Derived Rain Rates Estimated by Neural Network in Convective Environments: A Study over Italy, Remote Sensing, 16, https://doi.org/10.3390/rs16101769, 2024.

Tridon, F., Battaglia, A., Rizik, A., Scarsi, F. E., and Illingworth, A.: Filling the Gap of Wind Observations Inside Tropical Cyclones, Earth and Space Science, 10, e2023EA003 099, https://doi.org/https://doi.org/10.1029/2023EA003099, e2023EA003099 2023EA003099, 2023.

Varlas, G., Pytharoulis, I., Steeneveld, G.-J., Katsafados, P., and Papadopoulos, A.: Investigating the impact of sea surface temperature on the development of the Mediterranean tropical-like cyclone “Ianos” in 2020, Atmospheric Research, 291, 106 827, https://doi.org/https://doi.org/10.1016/j.atmosres.2023.106827, 2023.